



This is a repository copy of *Therapeutic vulnerabilities in the DNA damage response for the treatment of ATRX mutant neuroblastoma*.

White Rose Research Online URL for this paper:
<http://eprints.whiterose.ac.uk/165031/>

Version: Published Version

Article:

George, S.L., Lorenzi, F., King, D. et al. (14 more authors) (2020) Therapeutic vulnerabilities in the DNA damage response for the treatment of ATRX mutant neuroblastoma. *EBioMedicine*, 59. 102971. ISSN 2352-3964

<https://doi.org/10.1016/j.ebiom.2020.102971>

Reuse

This article is distributed under the terms of the Creative Commons Attribution-NonCommercial-NoDerivs (CC BY-NC-ND) licence. This licence only allows you to download this work and share it with others as long as you credit the authors, but you can't change the article in any way or use it commercially. More information and the full terms of the licence here: <https://creativecommons.org/licenses/>

Takedown

If you consider content in White Rose Research Online to be in breach of UK law, please notify us by emailing eprints@whiterose.ac.uk including the URL of the record and the reason for the withdrawal request.



eprints@whiterose.ac.uk
<https://eprints.whiterose.ac.uk/>



Research paper

Therapeutic vulnerabilities in the DNA damage response for the treatment of *ATRX* mutant neuroblastoma



Sally L George^{a,b,*}, Federica Lorenzi^a, David King^c, Sabine Hartlieb^d, James Campbell^e, Helen Pemberton^f, Umut H Toprak^d, Karen Barker^a, Jennifer Tall^a, Barbara Martins da Costa^a, Marlinde L van den Boogaard^g, M Emmy M Dolman^g, Jan J Molenaar^g, Helen E Bryant^c, Frank Westermann^d, Christopher J Lord^f, Louis Chesler^{a,b}

^a Paediatric Tumour Biology, Division of Clinical Studies, The Institute of Cancer Research, Sutton, Surrey SM2 5NG, United Kingdom

^b Children and Young People's Unit, Royal Marsden NHS Foundation Trust, Sutton, Surrey SM2 5PT United Kingdom

^c Academic Unit of Molecular Oncology, Sheffield Institute for Nucleic Acids (SInFoNIA), Department of Oncology and Metabolism, University of Sheffield, Beech Hill Road, Sheffield S10 2RX, United Kingdom

^d Neuroblastoma Genomics, Hopp Children's Cancer Center Heidelberg (KITZ) & German Cancer Research Center (DKFZ), Heidelberg, Germany

^e Bioinformatics Core Facility, The Institute of Cancer Research, London, United Kingdom

^f CRUK Gene Function Laboratory and Breast Cancer Now Toby Robins Research Centre, Institute of Cancer Research London, SW3 6JB, United Kingdom

^g Princess Maxima Center for Pediatric Cancer, Utrecht, The Netherlands

ARTICLE INFO

Article History:

Received 22 May 2020

Revised 7 August 2020

Accepted 7 August 2020

Available online xxx

Keywords:

Neuroblastoma

ATRX

DNA damage response

PARP

ABSTRACT

Background: In neuroblastoma, genetic alterations in *ATRX*, define a distinct poor outcome patient subgroup. Despite the need for new therapies, there is a lack of available models and a dearth of pre-clinical research.

Methods: To evaluate the impact of *ATRX* loss of function (LoF) in neuroblastoma, we utilized CRISPR-Cas9 gene editing to generate neuroblastoma cell lines isogenic for *ATRX*. We used these and other models to identify therapeutically exploitable synthetic lethal vulnerabilities associated with *ATRX* LoF.

Findings: In isogenic cell lines, we found that *ATRX* inactivation results in increased DNA damage, homologous recombination repair (HRR) defects and impaired replication fork processivity. In keeping with this, high-throughput compound screening showed selective sensitivity in *ATRX* mutant cells to multiple PARP inhibitors and the ATM inhibitor KU60019. *ATRX* mutant cells also showed selective sensitivity to the DNA damaging agents, sapacitabine and irinotecan. HRR deficiency was also seen in the *ATRX* deleted CHLA-90 cell line, and significant sensitivity demonstrated to olaparib/irinotecan combination therapy in all *ATRX* LoF models. *In-vivo* sensitivity to olaparib/irinotecan was seen in *ATRX* mutant but not wild-type xenografts. Finally, sustained responses to olaparib/irinotecan therapy were seen in an *ATRX* deleted neuroblastoma patient derived xenograft.

Interpretation: *ATRX* LoF results in specific DNA damage repair defects that can be therapeutically exploited. In *ATRX* LoF models, preclinical sensitivity is demonstrated to olaparib and irinotecan, a combination that can be rapidly translated into the clinic.

Funding: This work was supported by Christopher's Smile, Neuroblastoma UK, Cancer Research UK, and the Royal Marsden Hospital NIHR BRC.

© 2020 The Authors. Published by Elsevier B.V. This is an open access article under the CC BY-NC-ND license.

(<http://creativecommons.org/licenses/by-nc-nd/4.0/>)

1. Introduction

Neuroblastoma, a tumour of the peripheral sympathetic nervous system is a common, poor outcome tumour of childhood. Half of patients have clinical high-risk disease at the time of diagnosis, defined as age greater than 18 months, the presence of distant

metastases and/or amplification of the *MYCN* oncogene [1]. Despite intensification of conventional therapies in recent years approximately half of all children with high-risk neuroblastoma still die with relapsed/refractory disease [2–4].

Recent studies have found that the majority of poor outcome neuroblastoma can be subdivided into three mutually exclusive molecular subgroups defined by: *MYCN* amplification (37%), telomerase reverse transcriptase (*TERT*) rearrangements (23%) and alpha thalassaemia mental retardation X-linked (*ATRX*) mutations or deletions (11%) [5,6]. With putative roles in the genesis of biologically

* Corresponding author.

E-mail address: Sally.George@icr.ac.uk (S.L. George).

Research in context

Evidence before this study

ATRX has been shown to have differing roles in the regulation of DNA damage repair in different cell line and murine models, hence it has been suggested that DNA damage response inhibitors may have a role in selectively targeting some *ATRX* mutant cancers. *ATRX* mutations are enriched in poor outcome paediatric tumours, and specifically in neuroblastoma are associated with a chronic refractory phenotype and poor survival. Novel therapies are urgently needed for this group of patients.

Added value of this study

We show that in neuroblastoma models, *ATRX* loss of function results in impairment of DNA damage repair by homologous recombination and impaired replication fork processivity. In keeping with this, using a screen of over 400 compounds, we identify PARP inhibitors as the most significant hit showing selective sensitivity in *ATRX* mutant cells. We then demonstrate that the combination of the PARP inhibitor olaparib with the DNA damaging agent irinotecan is effective in pre-clinical neuroblastoma models with genetic alterations in *ATRX*.

Implications of all the available evidence

Our pre-clinical data supports the development of clinical trials of PARP inhibitor combination therapy for children with neuroblastoma associated with genetic alterations in *ATRX*.

aggressive disease, these genomic alterations represent attractive therapeutic targets for high-risk neuroblastoma. In particular, the *ATRX* subgroup of neuroblastoma patients has a distinct clinical phenotype, with an older age at diagnosis, conventional therapy resistance and a chronic but progressive disease course [7], reinforcing the notion that alterations in *ATRX* function underlie the unique behaviour of these tumours. In support of this, *ATRX* is the third most commonly mutated gene across all paediatric malignancies, and recurrently mutated in poor outcome tumours such as high-grade glioma and osteosarcoma [8]. Taken together these data indicate that LoF alterations in *ATRX* are a likely driver of paediatric cancer biology, emphasizing the urgent need to develop effective therapeutic strategies for *ATRX* mutated cancers.

Numerous functions of *ATRX* could underlie the prominent role of this gene in cellular biology of these cancers. *ATRX* plays an important role in transcriptional regulation by extensive and not yet completely understood mechanisms. *ATRX* is enriched at the silenced allele of imprinted regions. It is also known to regulate gene transcription via binding to the H3K9me3 mark and also via binding to and the resolution of G-quadruplex structures [9–11]. *ATRX* also orchestrates histone 3.3 deposition within telomeres, and pericentric DNA, thus maintaining genomic stability in these repetitive regions [12,13]. Concordant with this, *ATRX* LoF is the strongest predisposing factor associated with the development of the recombination mediated telomere synthesis mechanism: alternative lengthening of telomeres (ALT) [14].

ATRX has also been implicated in the regulation of DNA damage repair (DDR) both by non-homologous end joining (NHEJ) and homologous recombination repair (HRR). DDR reporter plasmid assays have shown that *ATRX* knockdown by shRNA in murine glial cells results in impairment of NHEJ but not HRR [15]. However, in cancer cell line models siRNA down-regulation of *ATRX* has been shown to result in impairment of RAD51 localization to BRCA1, a key trigger for HRR signalling [16].

In summary the *ATRX* gene has multiple functions that may underlie the ability of LoF alterations to influence both disease pathogenesis and the response to therapeutic agents.

Specifically in neuroblastoma, the commonest genetic alterations seen are either large multi-exon deletions encompassing the ADD domain or mutations clustering around the Helicase C-terminal region [7,17]. As in other cancers, both of these alterations are thought to result in disruption of normal *ATRX* function, however recently it has been shown that *ATRX* deletions also result in the formation of a truncated in frame fusion protein which redistributes to promoters of active genes [18].

Here we generated isogenic models of *ATRX* mutant neuroblastoma for mechanistic interrogation, then took an unbiased approach using high throughput compound screening, in order to identify which of these potential mechanisms are therapeutically exploitable. We then validated findings in neuroblastoma models with *ATRX* deletions/in frame fusions, with the ultimate aim of identifying rapidly translatable novel therapeutic strategies for this poor outcome group of patients.

2. Materials and methods

2.1. Cell lines

The SKNSH cell line was obtained from ATCC and cultured in Dulbecco's Modified Eagle Medium, supplemented with 10% foetal bovine serum (Thermo Fisher). The CHLA-90 cell line was obtained from the Children's Oncology Group Cell Line Repository and cultured in Iscove's Modified Dulbecco's Medium supplemented with 20% foetal bovine serum (Thermo Fisher). Both cell lines were verified by short tandem repeat DNA profiling and confirmed to be mycoplasma free using the LookOut[®] mycoplasma PCR detection kit.

2.2. CRISPR Cas9 gene editing

NickaseNinja CRISPR Cas9 constructs (DNA 2.0) were designed using the company's gRNA design tool and checked to ensure target specificity, using the Basic Local Alignment Search Tool (BLAST[®] - <https://blast.ncbi.nlm.nih.gov>). The TP53 gRNA was designed to target exon 3 and the *ATRX* gRNA to target the helicase C terminal domain. Twenty-four hours following transfection with the *ATRX* CRISPR Cas9 plasmid or the TP53 CRISPR Cas9 plasmid, single cells expressing RFP-Paprika or GFP (depending on the construct) were FACS sorted into 96 well plates and then expanded to create stable TP53 and *ATRX* knockout cell lines.

2.3. Generation of AMC-772 PDX model

The AMC-772 organoid was established as previously described [19] and then used to establish a xenograft model. Ethical approval was obtained under project number AVD3990020173068, study protocol PMC.63.3068.1801. 4.3×10^6 AMC772T cells were xenografted into both flanks of four NMRI nu-/nu- mice at 6–8 weeks of age. tumour size was monitored twice a week by calliper measurements and determined using the formula $(\pi/6)d^3$. Once the tumour reached 1500 mm³ in size, tumors were passaged to 3 NMRI nu-/nu- mice at 6–8 weeks of age. Once the tumour reached 1500 mm³ in size, tumors were cut in pieces and cryopreserved in 10% DMSO for xenotransplantation in recipient mice.

2.4. Animal experiments

Mice were subcutaneously injected unilaterally with 1×10^6 cells to obtain Passage 0 (P0) xenografts. To improve the latency, xenografts of both p53(2) and E6 cells were dissociated into single cells and re-injected into NSG mice twice. P2 xenografts were used for the pre-clinical trial. AMC-772 P2 xenografts were supplied frozen from The Princes Maxima centre and passaged once. Calipers were used to measure tumour diameter on two axes, 2–3 times per week. 4–6

animals were enrolled onto each treatment arm once the tumour size reached 5–10 mm. Studies were terminated when the mean diameter of the tumour reached 15 mm. Doses administered were: olaparib 50 mg/kg twice daily for 2 weeks, irinotecan 1.35 mg/kg daily for 2 weeks, temozolomide 8 mg/kg for 1 week. All experimental protocols were approved and monitored by The Institute of Cancer Research Animal Welfare and Ethical Review Body (PPL 70/7945, later PPL P91E52C32), in compliance with the UK Home Office Animals (Scientific Procedures) Act 1986. Antibodies used for immunohistochemistry were: ATRX (Santa Cruz, sc-55,584), Ki67 (BD biosciences, 556,003).

2.5. Immunofluorescence and immunoblotting

Immunoblotting for ATRX and p53, and Immunofluorescence for phosphorylated histone H2AX^(ser139) (γ H2AX) foci was performed in untreated cells. Immunofluorescence for RAD51/BRCA1 and γ H2AX/DNAPK^(ser2056) was performed at eight hours and 30 minutes respectively post irradiation (10 gray), or 24 h following the addition of 5 μ M irinotecan. Antibodies used for immunofluorescence and immunoblotting studies were: ATRX (Sigma - HPA001906), GAPDH (Cell signalling - 2118), phospho-H2AX^(ser139) (Cell signalling - 76,310), PARP (Cell signalling - 9532), HRP conjugated p53 (R&D systems - HAF1355), BRCA1 (Santa Cruz - sc6954), RAD51 (Abcam - ab63801), DNAPK^(ser2056) (Cell signalling - 12,311).

2.6. DNA fibre assay

7.5×10^6 cells were seeded and left to attach for at least four hours before labelling with a 25 μ M CldU pulse for 20 min, then either left untreated or exposed to 4 mM HU +/- 50 μ M mirin for five hours. Cells were trypsinised and re-suspended in cold PBS to a final volume of 4×10^5 cells/ml. 2 μ L of cells were mixed with 7 μ L of spreading buffer (200 mM Tris-HCl, pH 7.4, 50 mM EDTA, and 0.5% SDS) on a glass slide, incubated for two minutes, then tilted 15–45° to allow the DNA spreads to run down the slide, then air dried, fixed in 3:1 methanol:acetic acid, and refrigerated overnight.

DNA fibres were then denatured in 2.5 M HCl for one hour, washed with PBS, and blocked with 1% BSA in PBS-T (PBS and 0.1% Tween 20) for one hour. CldU DNA tracts were labelled for one hour with 1:1000 rat α -BrdU (Biorad, UK) rinsed with PBS and the secondary antibody was applied (α -rat AlexaFluor 555 at 1:500). After further PBS washes, coverslips were applied using Vectashield (Vector Laboratories) and slides stored at -20 °C. The DNA fibres were visualised using an Olympus FV1000 confocal microscope with a PLAPON 60x oil objective lens and a laser of 542 nm wavelength. DNA fibre lengths were measured in ImageJ (Bethesda, MD, USA). Indicated numbers of labelled DNA fibres from three independent experiments per condition were imaged.

2.7. High throughput compound screening

Compounds were obtained from multiple sources including collections from MicroSource Discovery Systems, Inc (US Drug Collection), ENZO Life Sciences (FDA approved Library, BML-2841), Prestwick Chemical (Prestwick Chemical Library®) and a collection of commercially available signal transduction inhibitors. Library 1 contains 390 compounds tested at 4 dose levels with a maximum dose of 0.5 μ M. Library 2 contains 80 compounds tested at 8 dose levels with a maximum dose of 1 μ M, (Table S1 and S2). Wells containing 0.2% DMSO, were used as a control for viability, and vials containing 2 μ g/ml puromycin were used as a control for cell death.

Both screens contained 2 independent replicates of the SKNSH cell line and the isogenic cell lines generated from SKNSH by CRISPR Cas9 deletion of *TP53* and *ATRX* named: p53(2) (*TP53* mutant), A3, E1 and E6 (generated from p53(2), mutant for both *TP53* and *ATRX*). 500 cells

per well were plated in opaque 384 well plates and after 24 h of incubation compounds were then added in triplicate for each dose level. After 5 days incubation, cell viability assessed by Cell Titre Glo®. Pearson's correlation between normalised values for each replicate was between 0.94 and 1. For each compound AUC was calculated using the drc R-package as a read out for drug sensitivity.

Linear mixed effects models were used to test for differences in AUC for each compound dependant on *ATRX* gene status. Fixed effects (*ATRX* gene status) and random effects (replicate screen for each cell line) were coded as factors and the drc R-package was used to fit models. Compounds where the fixed effect (*ATRX* gene status) was nominally significant (uncorrected p-value ≤ 0.05) were selected. In addition, we focused on those compounds where the magnitude of the difference between the wild type and *ATRX* mutant group was greatest, specifically focusing on those compounds where the difference in AUC between the wild type and *ATRX* mutant groups were greater than 0.1 (with 1.0 being the maximum AUC corresponding to no inhibition of growth).

2.8. Sequencing

WGS was done at the Genomic and Proteomics sequencing core facility at the German Cancer Research centre (DKFZ), Heidelberg, Germany. DNA was isolated using the Invitrogen PureLink® DNA mini kit according to manufacturer's instructions. Library preparation was done using the Truseq DNA Nano kit (Illumina) and libraries were size selected using SPRI beads (Beckman Coulter Genomics). Samples were sequenced on the Illumina HiSeq X Ten platform using 150 bp paired end sequencing with 60 X coverage. Samples were aligned by the One Touch Pipeline (OTP) service at the German Cancer Research centre (DKFZ). WGS data was aligned to the 1KGRF_PhiX reference genome using BWA-MEM version 0.7.15 (option -T 0). Sambamba version 0.6.5 was used for merging and duplication marking. Samtools version 0.1.19 was used to filter and sort the bam files. This in-house workflow was recently described in detail by Jabs. et al. [20]. NGS Panel sequencing was analysed as previously reported [21].

2.9. SF₅₀ experiments

SF₅₀ experiments were performed in 96 well plate format. The number of cells used for each SF₅₀ experiment was determined in a prior experiment to evaluate the number of cells necessary to reach 70–90% confluency by the desired time-point. Cells were seeded into 96-well plates and the following day compound was added to wells in triplicate, across a concentration gradient including one three well replicate of DMSO-only controls. At the relevant time point cell viability was assessed by Cell titre Glo® assay. The SF₅₀ was calculated as the drug concentration that inhibits viability/cell growth by 50% compared with controls, according to non-linear regression analysis, using Graphpad Prism. Olaparib, rucaparib, talazoparib, KU60019 irinotecan and temozolomide were purchased from SelleckChem, Sapa-citabine was purchased from AdooQ Bioscience.

2.10. PARP siRNA

Two different ON-TARGETplus siRNAs targeting PARP1 (#J-006,656-06-0002 and #J-006,656-07-0002) and a non-targeting control siRNA (#D-001,810-01-05) were purchased from Dharmacon. Cells were transfected with Dharmacon 1 transfection agent as per the manufacturers instructions. PARP1 downregulation was assessed by western blotting and cell viability by Cell titre Glo® assay. Survival in cells following PARP1 knockdown was normalized to the non-targeting control siRNA.

2.11. Pharmacodynamic assays

The HT PARP *in-vivo* pharmacodynamic assay kit (Trevigen) was utilized to quantify PAR levels as per manufacturers instructions. For the CHLA90 cell line the assay was performed 24 h after treatment with vehicle versus 1 μ M olaparib. For *in-vivo* studies, PAR levels were quantified one hour after administration of either 50 mg/kg olaparib or vehicle.

2.12. Statistical analyses and data

All results are expressed as mean \pm standard deviation unless otherwise indicated. Statistical analysis of compound screen data using linear mixed effects models was done using the R package as indicated above. All other statistical analysis was done using graphpad prism version 7.

2.13. Role of funding source

Financial support for this work was provided by the charities Christopher's Smile, Neuroblastoma UK, Cancer Research UK, and the Royal Marsden Hospital NIHR BRC. None of these organizations had any role in the study design, data collection, data analyses, interpretation, or writing of report.

3. Results

3.1. ATRX CRISPR Cas9 knock-out in neuroblastoma cell lines results in HRR deficiency and impairment of replication fork processivity

In neuroblastoma, ATRX alterations and ALT are mutually exclusive with MYCN amplification [22]. In order to identify biologically relevant models of neuroblastoma we evaluated a panel of 7 MYCN non-amplified neuroblastoma cell lines for ATRX protein expression and telomerase activity (Fig. S1 a-b). The SKNSH cell line was selected for ATRX gene editing as it expresses high levels of ATRX, and does not display the ALT phenotype. The only other cell line identified fulfilling these criteria was NBL-S, however this cell line is known to express high levels of MYCN [23].

We surmised that generation of stable ATRX-deleted cells would require prior p53 inactivation, given that ALT neuroblastoma cell lines frequently show p53 pathway aberrations [24], CRISPR Cas9 gene-editing activates p53-mediated DNA damage repair in differentiated cells [25], and that ATRX loss results in p53-driven apoptotic cell-death in neural progenitors [26]. Indeed, ATRX knockout via CRISPR Cas9 was lethal in TP53 wild type SKNSH cells (Fig. S1 c-e), and as expected [25,26] drove high-levels of apoptosis in TP53 wild type cells (Fig. S1f). However, with prior deletion of TP53, we generated three stable cell lines by CRISPR Cas9 ATRX gene editing (named as A3, E1 and E6) that were devoid of ATRX expression (Fig. 1a). Whole genome sequencing (WGS) confirmed presence of the small indels in the targeted region of TP53, and differing indels in the targeted region of ATRX in the A3, E1 and E6 clones (Table S1, Fig. S1h).

In untreated ATRX mutant cell lines we observed an increase in the number of γ H2AX foci (Fig. 1b-c), suggesting an increase in stalled and collapsed replication forks. Given that ATRX plays a key role in the regulation of DNA damage repair pathways, we asked whether the increase in γ H2AX could represent a failure to effectively repair DNA lesions due to a defect in activation of canonical double stranded DNA repair mechanisms: NHEJ and HRR. Induction of DNA damage via ionizing irradiation resulted in auto-phosphorylation of DNA dependant protein kinase (DNA-PK^(ser2056)) and localization to sites of DNA damage in both ATRX wild type and mutant cells (Fig. 1d-e), this suggests that ATRX mutant cells are still proficient in the initiation of DNA repair by NHEJ [27]. Conversely, ATRX mutant cells exhibited a clear loss of RAD51 and BRCA1 co-localization, an

indicator of defective homologous recombination (Fig. 1f-g). In view of these findings, we assessed WGS data for off-target mutations in genes with known roles in HRR that could explain the observed HRR deficiency in the CRISPR Cas9 edited isogenic cell lines (Table S1). This confirmed no off-target exonic variants or indels in any of the CRISPR Cas9 generated cell lines, suggesting the ATRX LoF mutations could be the cause of the RAD51 defect. WGS data were also used to generate homologous recombination deficiency (HRD) scores [28]. There was no significant increase in the overall score in ATRX mutant cell lines, but one of the contributing parameters: the number of telomeric allelic imbalance events was increased in the ATRX mutant lines (Table S1), in keeping with the known role of ATRX in telomere maintenance [29] and also indicative of DNA repair deficiencies [30].

The ability to faithfully replicate DNA is another key hallmark of genomic integrity and both p53 and ATRX are reported to protect stalled replication forks [16,31]. We evaluated mean DNA fibre length, as a marker of replication fork processivity. As expected TP53 knockout resulted in a significantly lower mean DNA fibre length and this was further enhanced by mutation of ATRX (Fig. 2a-d). In the presence of hydroxyurea induced replication stress, all three cell lines exhibited shortened fibre lengths compared to untreated cells suggesting increased fork stalling as would be expected. However the degree of shortening was far greater in ATRX mutant cells compared to the other cell lines. This suggests that ATRX either reduces stalling or has a protective role at stalled forks. In keeping with the ability of ATRX to bind to and inhibit MRE11, an exonuclease that degrades stalled forks following DNA damage [16] the MRE11 inhibitor mirin was able to reverse the effects on fibre lengths only in the ATRX mutant cells (Fig. 2e-g). This strongly suggests that ATRX mediates MRE11-dependant degradation at stalled replication forks in the context of neuroblastoma.

Taken together, these data indicate that ATRX plays an important role in maintenance of DNA / genome integrity in neuroblastoma cells, through regulation of DNA repair mechanisms and maintenance of replication fork stability.

3.2. High-throughput small molecule inhibitor screening identifies specific ATRX dependant DNA damage repair pathway vulnerabilities and PARP inhibitor sensitivity

To identify therapeutic sensitivities relating to ATRX deficiency, we performed high-throughput small molecule inhibitor sensitivity screens using compound libraries containing inhibitors of DNA repair, in addition to a broad range of conventional chemotherapy agents and small molecules that target wide-ranging, cancer relevant pathways. The panel of isogenic cell lines varying in ATRX and TP53 status was screened with two clinical compound libraries. A broad screen containing 390 compounds tested at 4 dose levels (screen 1) and a narrower but more sensitive screen containing 80 compounds tested at 8 concentrations (screen 2) (Table S2).

Of the 390 distinct compounds tested in screen 1, three compounds met the criteria for ATRX synthetic lethality. This was arbitrarily defined as both a statistically significant difference in AUCs between the wild type and ATRX mutant groups, and a difference in mean AUCs between the wild type and ATRX mutant groups of greater than 0.1 (Fig. 3a). The strongest hit identified was the clinical poly-(ADP-Ribose) polymerase (PARP) inhibitor talazoparib [32]. No clear sensitivity patterns were identified for other modulators of DNA damage repair (Fig. S2a). The other compounds identified with selective sensitivity were the heat shock protein 90 (HSP 90) inhibitor: 17-AAG [33], and the amino-peptidase inhibitor tosedosat [34]. Fourteen compounds met the criteria for selective resistance in the ATRX mutants, including three different histone deacetylase (HDAC) inhibitors and two different aurora kinase inhibitors, where a clear trend towards relative resistance was identified for multiple compounds from both classes of agent (Fig. 3a, Fig. S2b).

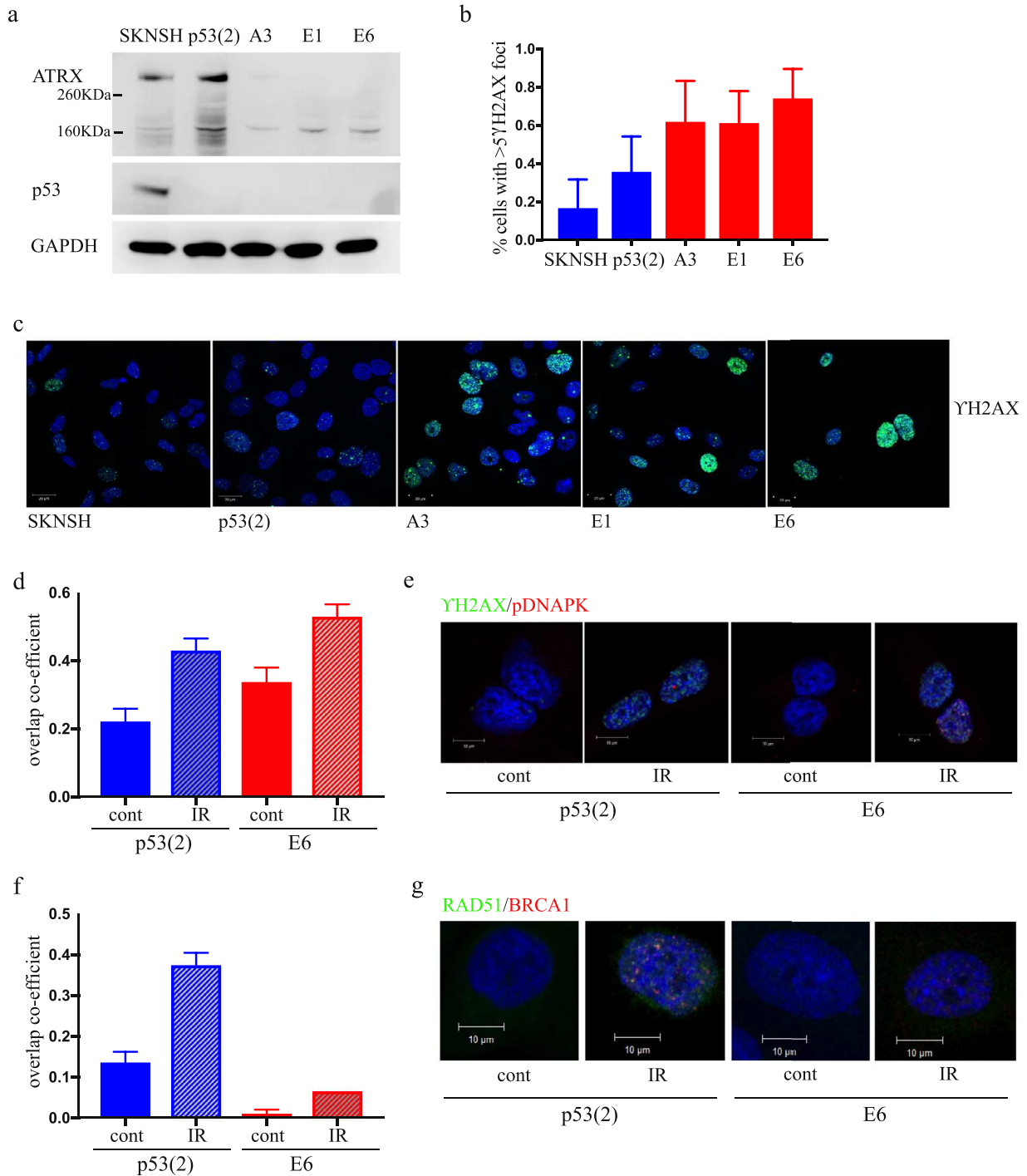


Fig. 1. Generation of stable ATRX CRISPR Cas9 knock-out neuroblastoma cell lines results in increased DNA damage and HRR deficiency. (a) Western blot showing ATRX and p53 expression in the isogenic panel of cell lines generated by CRISPR Cas9 gene editing of SKNSH (b) Proportion of untreated cells with >5 γ H2AX foci (error bars represent SD from 2 independent experiments, minimum 140 cells, $p < 0.0001$ by one-way Anova). (c) Representative images showing γ H2AX foci in untreated cells. (d) Quantification of the overlap coefficient of γ H2AX and pDNA PK foci by immunofluorescence, 30 min post 10 Gy irradiation (IR) versus control (cont), in p53(2) and E6 cell lines (e) Representative images from pDNA PK (red) and γ H2AX (green) co-localisation experiment. (f) Quantification of the overlap coefficient of BRCA1 and RAD51 foci by immunofluorescence, 8 hours post 10 Gy IR versus cont, in p53(2) and E6 cell lines. (g) Representative images from BRCA1 (red) and RAD51 (green) co-localisation experiment. For co-localisation experiments a minimum of 100 cells from 2 experiments were analysed by the ZEN software co-localisation analysis tool. Error bars represent SEM.

In screen 2, nine distinct compounds met the criteria for selectivity. In all cases the significant differences in AUC represented greater sensitivity in the ATRX mutant group relative to the wild-type group (Fig. 3b). Of the nine distinct compounds identified as selective against the ATRX mutants, five of these implicated vulnerabilities in DNA damage repair mechanisms (Fig. 3b, Fig S3a). Selective sensitivity to all three clinical PARP inhibitors contained

in the screen was identified (talazoparib, rucaparib and olaparib) and independently verified (Fig 3b, Fig S3 b-d, g). The ATRX mutants also showed selective sensitivity to the toolbox ataxia telangiectasia mutated (ATM) inhibitor KU60019 and to sapacitabine, an inducer of DNA double strand breaks known to be effective in models of HR deficient cancer (Fig. 3b, Fig S3 e-g) [35]. Aside from inhibitors of the DNA damage response, additional

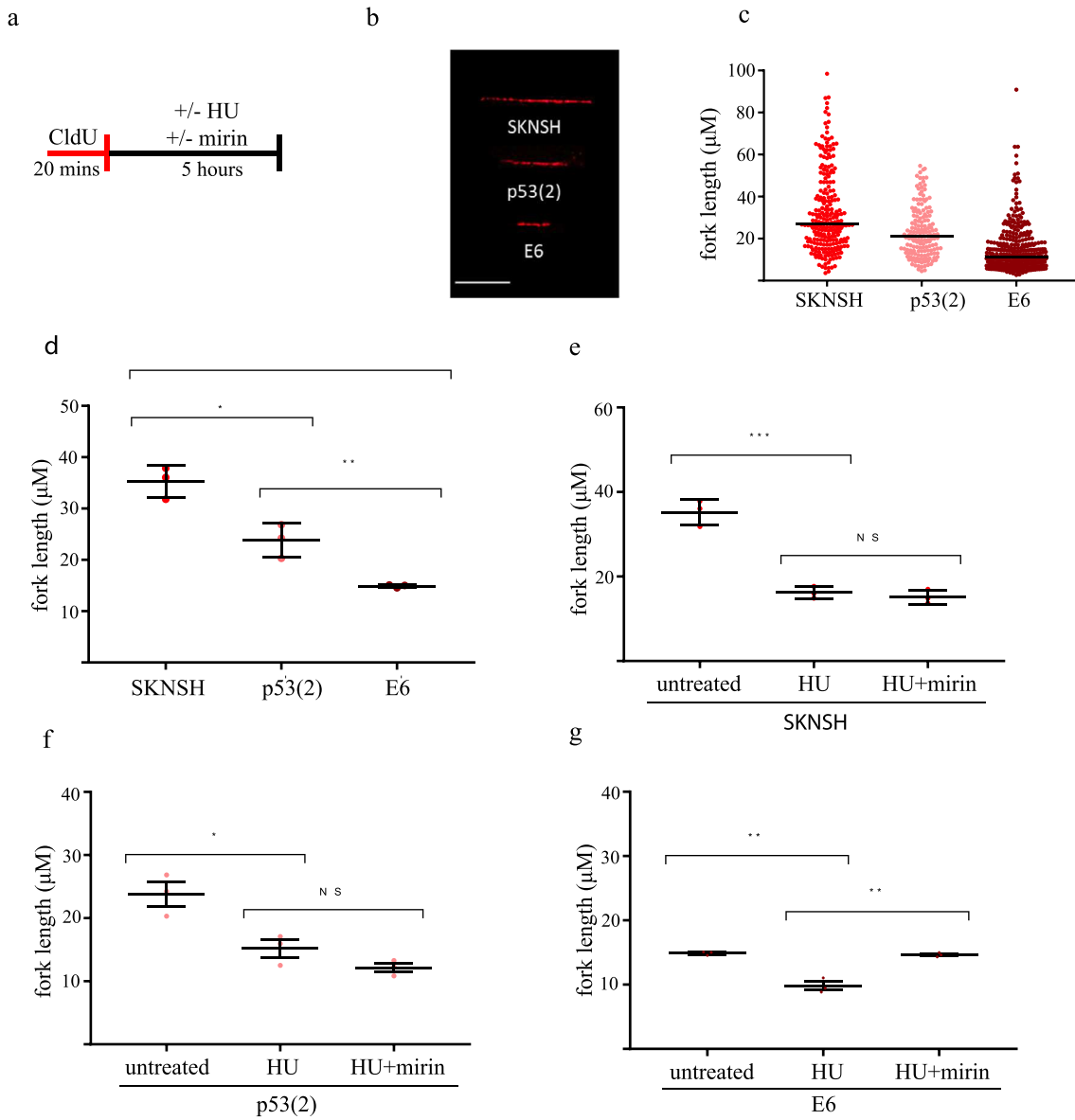


Fig. 2. ATRX facilitates replication fork processivity and fork protection in neuroblastoma cells. (a) SKNSH, p53(2) and E6 cells were pulsed with CldU and subsequently exposed to hydroxyurea (HU) and mirin for five hours as indicated in the schematic. (b) Representative fibre images (c) Distribution of DNA fibre length for untreated cells together with (d) mean fibre length. p53 knockout results in significantly reduced mean DNA fibre length which is further reduced with loss of ATRX. Data pooled from three independent repeats to show the distribution of DNA fibre length with the median indicated by the black line. Total fibres counted are as follows: SKNSH ($n = 241$), p53- ($n = 165$), ATRX- ($n = 350$). The data for mean fibre length are presented as the mean \pm SEM for three independent repeats. Response of (e) SKNSH, (f) p53(2) and (g) E6 cells to HU treatment alone or with mirin. The data for mean fibre length are presented as the mean \pm SEM for three independent repeats. Significance determined by student's unpaired t -test where *** $p < 0.001$, ** $p < 0.01$, * $p < 0.05$.

compounds identified by the screen with a high degree of preferential sensitivity in the *ATR*X mutants were the multi-tyrosine kinase inhibitor sunitinib [36] and, in keeping with screen 1, the HSP 90 inhibitor: 17-AAG [33].

Taken together, the combined findings from both screens indicate specific vulnerabilities in DNA damage repair in the *ATR*X mutants, with broad class specific sensitivity identified to PARP inhibitors. In keeping with this, genetic knockdown of PARP-1 also reduced cell viability in *ATR*X mutant cells in comparison with the parent cell line (Fig. 3c-d). We therefore focused on further pre-clinical evaluation of the PARP inhibitor olaparib as a therapeutic strategy for *ATR*X mutant neuroblastoma. This agent is already clinically approved in adult use and is in clinical trials for children so there is greater potential for rapid translation into the clinic for this indication.

3.3. PARP inhibition increases sensitivity to irinotecan in models of *ATR*X mutant neuroblastoma

In order to maximize the potential therapeutic benefit of PARP inhibition, we then evaluated compound screen data from the isogenic panel to identify potential candidate chemotherapy agents for combinatorial studies. Evaluation of compound screen data for sensitivity to chemotherapy agents commonly used at the time of neuroblastoma relapse showed no differences between the groups in sensitivity to temozolomide, topotecan or cyclophosphamide (Fig. S4a-c) but revealed that although loss of *TP53* results in irinotecan resistance, loss of *ATR*X re-sensitises cells to irinotecan (Fig. 4a). Preferential sensitivity to irinotecan in the *ATR*X mutant cells was subsequently verified, and combination therapy with olaparib evaluated (Fig. 4b). Although the addition of olaparib significantly

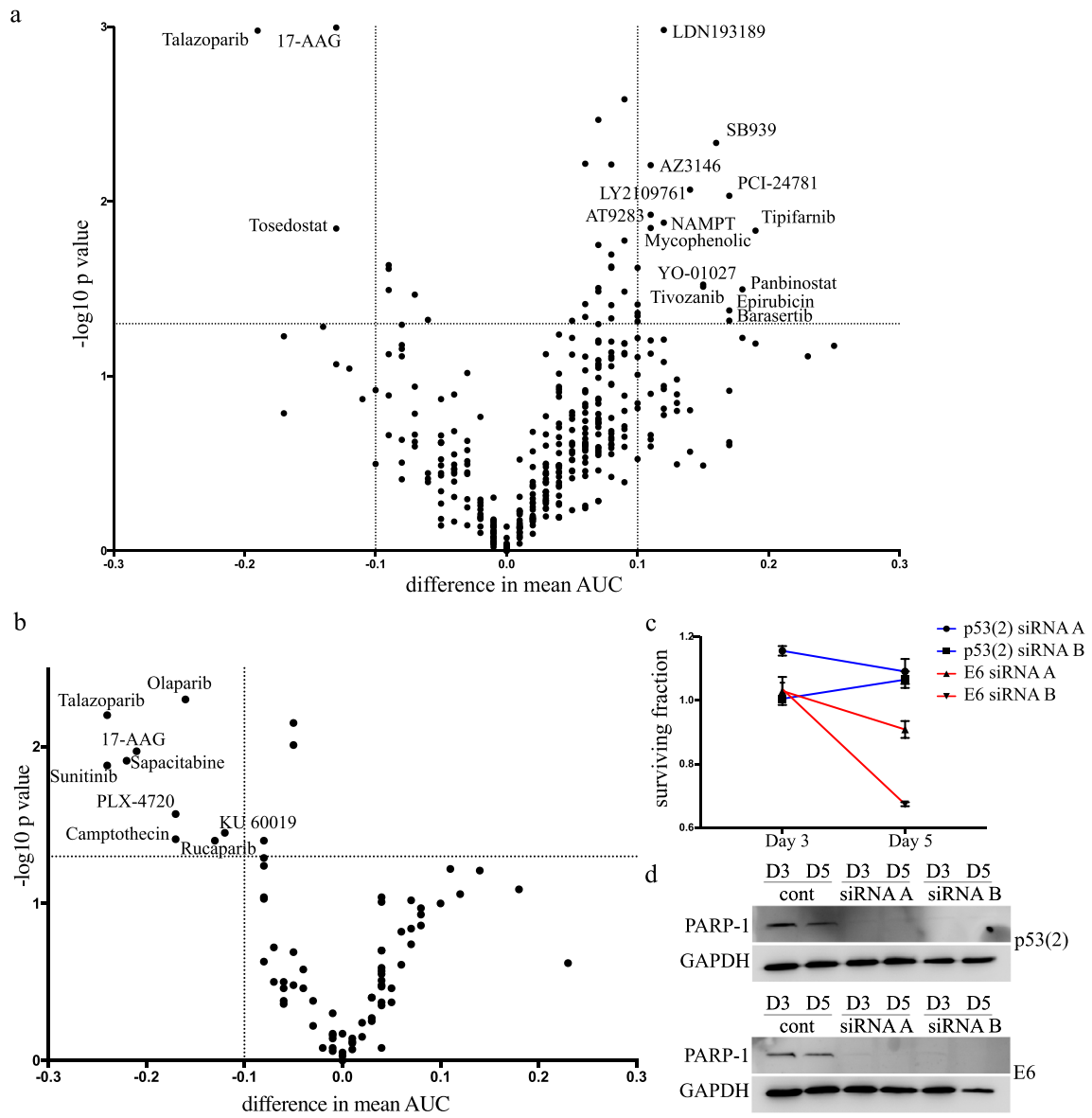


Fig. 3. Therapeutic screening identifies specific ATRX dependent DNA damage repair vulnerabilities and PARP inhibitor sensitivity. (a) Volcano plots showing the difference in mean AUC and the negative \log_{10} p-value of the difference in the AUC between the ATRX mutant and wild type groups for the 390 compounds tested in screen 1. Compounds fulfilling the criteria for selective sensitivity in the ATRX mutants are highlighted in the top left quadrant. Compounds fulfilling the criteria for selective resistance in the ATRX mutants are highlighted in the top right quadrant. (b) Volcano plots showing the difference in mean AUC and the negative \log_{10} p-value of the difference in the AUC between the ATRX mutant and wild type groups for the 80 compounds tested in screen 2 (c) Cell viability as measured by CellTiter-glo following genetic knockdown of PARP 1 with two different siRNAs, (normalized to control siRNA) in isogenic cell lines. (d) Western blot showing PARP 1 levels in same experiment as (c).

enhanced irinotecan sensitivity regardless of ATRX status, the cumulative sensitivity to the combination of irinotecan and olaparib was significantly greater in the ATRX mutants (Fig. 4b). Irinotecan stabilizes single strand breaks induced by topoisomerase 1 and is known to induce double strand DNA breaks through collapse of replication forks (37, 38). In keeping with impairment of HRR signalling at sites of irinotecan induced double stranded DNA damage, ATRX mutant cells were unable to co-localise RAD51 to BRCA1 following irinotecan therapy (Fig. 4c).

The failure of HRR signalling via the RAD51-BRCA1 co-localisation in response to irinotecan was also demonstrated in the ATRX deleted/in frame fusion cell line CHLA-90 (Fig. 4d-e). Finally, although CHLA-90 is relatively resistant to single agent olaparib the addition of olaparib at a low dose was sufficient to inhibit downstream PARP and significantly sensitized the CHLA-90 cell line to irinotecan (Fig. 4f and Fig. S4 d-f).

Taken together, this indicates that in neuroblastoma models, loss of normal ATRX function is associated with HRR deficiency and a lack of protection of stalled replication forks, thus sensitivity to PARP inhibition, particularly when combined with DNA damaging agents.

3.4. Olaparib and irinotecan therapy causes tumour regression in-vivo in ATRX mutant but not ATRX wild type xenografts

For *in-vivo* studies subcutaneous xenografts were established in NOD scid gamma (NSG) mice using the p53(2) and E6 cell lines. The median time from injection to tumour onset was significantly longer in the E6 xenografts in comparison with p53(2) xenografts (Fig. S5 a-b). Loss of ATRX expression seen in the E6 xenografts by immunohistochemistry (IHC) but Ki67 staining was seen in both xenografts (Fig. 5a). As published in preclinical Ewing sarcoma studies [39], pharmacodynamic inhibition of PARP activity in both

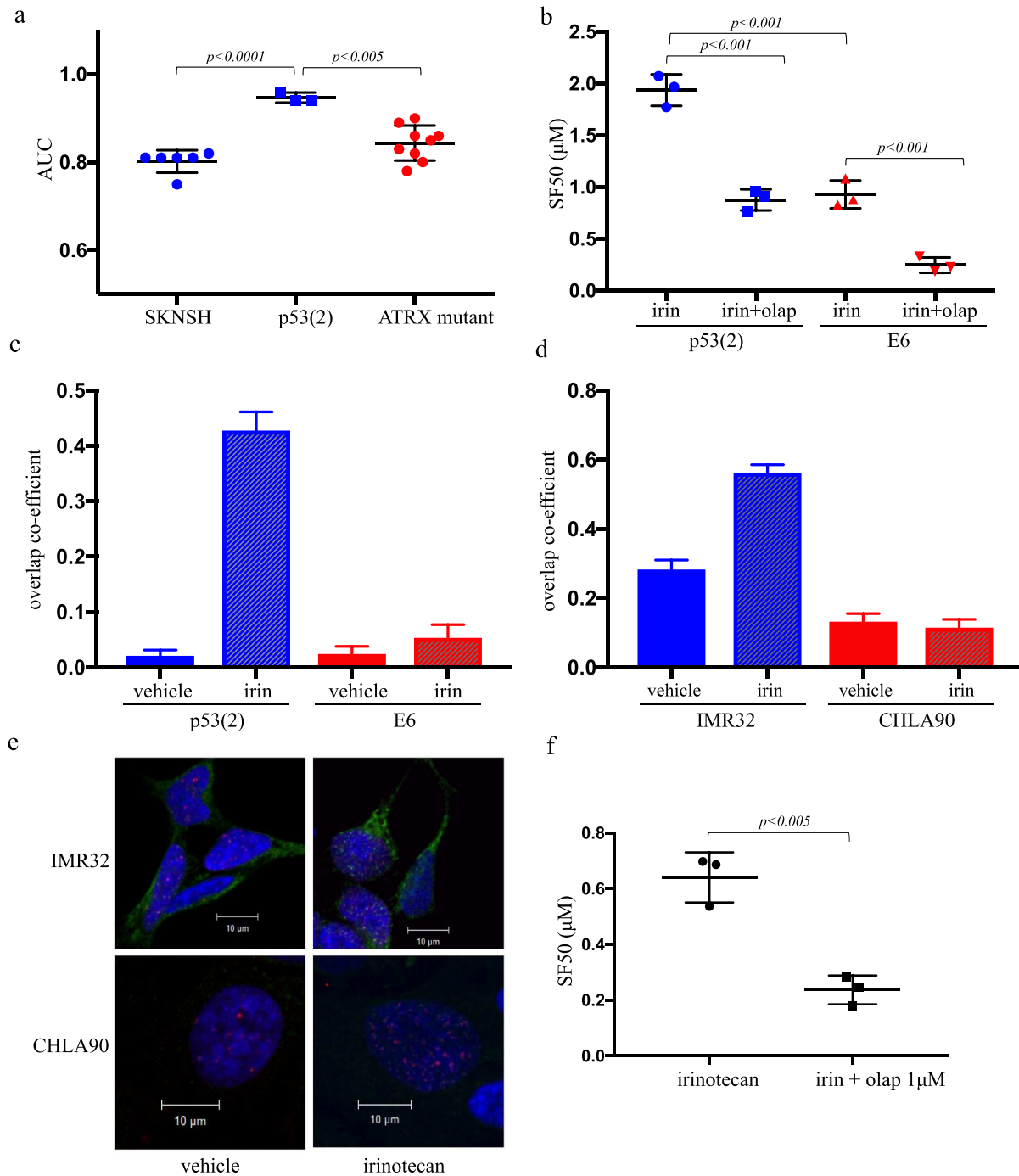


Fig. 4. PARP inhibition increases sensitivity to irinotecan in ATRX mutant neuroblastoma. (a) AUC scores for irinotecan from the compound screen, subdivided into *TP53* and *ATRX* status. (b) Summary of SF50 results for irinotecan alone or given in combination with 1 μM olaparib in *ATRX* wild type/mutant isogenic cell lines from 3 independent experiments. (c) Quantification of the overlap coefficient of BRCA1 and RAD51 foci by immunofluorescence, 24 h post irinotecan versus vehicle in p53(2) and E6 cell lines. (d) Quantification of the overlap coefficient of BRCA1 and RAD51 foci by immunofluorescence, 24 h post irinotecan versus vehicle in the CHLA90 cell line, compared with a *MYCN* amplified cell line. For (c) and (d), a minimum of 100 cells from 2 experiments were analysed by the ZEN software co-localisation analysis tool. Error bars represent SEM. (e) Representative images from BRCA1 (red) and RAD51 (green) co-localisation experiment from (d). (f) Comparison of the SF50 for irinotecan +/- olaparib 1 μM in the *ATRX* deleted cell line CHLA90, by three independent experiments, p value by unpaired students t-test.

p53(2) and E6 xenografts was confirmed at a dose of 50 mg/kg olaparib (Fig. 5b). On day 14 of olaparib/irinotecan combination therapy, tumour regression was observed in E6 xenografts but there was progressive disease in all treatment arms in the p53(2) xenografts (Fig. 5c-e, Fig. S5c-d). This translated into a small increase in survival in the E6 xenograft model following only 1 cycle of olaparib/irinotecan therapy (Fig. 5f-g).

Although all cell lines were highly resistant to temozolomide *in-vitro* (Fig. S6a), some sensitization to temozolomide was

demonstrated with the addition of olaparib, particularly in the E6 cell line (Fig. S6b). This, in combination with the fact that temozolomide is also used as standard backbone chemotherapy in relapsed neuroblastoma trials, prompted us to evaluate the combination of temozolomide and olaparib *in-vivo*. In contrast to single agent irinotecan, single agent temozolomide caused tumour regression in E6 xenografts. However, although the addition of olaparib to temozolomide did slow tumour growth, this did not translate to increased survival (Fig. S6).

induces proteasomal degradation of ATM [45,46]. Furthermore, BRCA1 deficient cells have been shown to be hypersensitive to 17AAG [47]. Taken together with the other findings in the screen, it is probable that 17AAG sensitivity in *ATRX* mutant cell lines, is at least in part a result of the downstream effects on the DNA damage response pathways.

In addition to identifying compounds that are selective for *ATRX* mutant cells, we also identified two classes of compound where there is relative resistance. HDAC inhibitors selectively kill cancer cells via inhibition of the many functions of HDAC proteins including chromatin remodelling and the modulation of gene transcription, which are thought to play a role in cancer development and progression [48]. The mechanism for relative HDAC resistance in the *ATRX* mutants is not certain but it may be that the resultant far-reaching epigenetic changes of *ATRX* LoF render HDAC mediated mechanisms less important for cancer cell survival. The mechanism of resistance to aurora kinase inhibitors is also unclear, although of note, both aurora kinase A and B has been shown to phosphorylate HDAC1. Therefore aurora kinase is implicated in the maintenance of HDAC enzymatic activity [49]. The relative resistance to aurora kinase inhibition identified by the screen is also in direct contrast with the preferential pre-clinical sensitivity of *MYCN* amplified neuroblastoma to aurora kinase A inhibitors [50], emphasizing the importance of molecular pre-selection for trials of novel agents in neuroblastoma patients.

The identification of specific DDR pathway vulnerabilities was the most significant finding from our screen. We decided to further validate PARP inhibition as a therapeutic strategy for *ATRX* mutant neuroblastoma, specifically olaparib, as a clinically available agent, which is already available in paediatric clinical trials, albeit for other indications. To maximise the potential clinical efficacy, rational combinations with standard therapies for relapsed neuroblastoma were sought. We identified preferential sensitivity to irinotecan in the *ATRX* mutants, which is in keeping with findings in an *in-vivo* model of *ATRX* LoF glioblastoma [15]. There is a strong rationale for this combination in other paediatric cancer models, where strong synergy between olaparib and irinotecan has been demonstrated [51], which we now also identify in neuroblastoma models.

Qadeer et al. recently reported that in neuroblastoma models with multi-exon *ATRX* deletions, an in frame fusion protein is expressed which activates RE1 Silencing Transcription Factor (*REST*), resulting in *EZH2* inhibitor sensitivity [18]. Of note we show HRR deficiency and olaparib/irinotecan sensitivity in both *ATRX* mutant and deletion/ in frame fusion neuroblastoma models. Therefore, this approach offers the opportunity for therapeutic targeting of loss of normal *ATRX* function in neuroblastoma regardless of the whether this results from a multi-exon deletion or frame-shift mutation.

In summary, we identify a distinct phenotype and clear differential compound sensitivity patterns following *ATRX* genetic deletion in a neuroblastoma model. Furthermore, we identify a rapidly translatable therapeutic approach for this poor outcome group of patients.

Author contributions

Conceptualization: SG, CL and LC. Methodology: SG, MB, MD, JM. Investigation: HP, SH, FW, FL, BC, JT, KB, HB, DK. Formal Analysis: JC, TU. Supervision: CL, LC. Writing-original draft: SG, FL, LC. Writing-review and editing: all authors

Data sharing

Whole genome sequencing data from the isogenic cell lines generated from SKNSH have been deposited on the European Genome-phenome archive and are available via the following links: <https://www.ebi.ac.uk/ega/studies/EGAS00001004550>: <https://www.ebi.ac.uk/ega/datasets/EGAD00001006294>:

All processed data from both drug screens is available in Table S3. Raw luminescence data from the screen is available on request.

Declaration of Competing Interest

Dr. Lord reports grants, personal fees and non-financial support from AstraZeneca, Merck KGaA, Artios and Vertex. Dr. Lord is also a named inventor on patents describing the use of DNA repair inhibitors and stands to gain from the development as part of the ICR "Rewards to Inventors" scheme. Dr Lord has received consultancy, SAB membership or honoraria payments from: Syncona, Sun Pharma, Gerson Lehrman Group, Merck KGaA, Vertex, AstraZeneca, Tango, 3rd Rock, Ono Pharma, Artios and has stock in Tango, Ovibio. This is outside the scope of the submitted work. Dr. Chesler reports grants from Christopher Smile Foundation, NIHR BRC, CRUK and the Neuroblastoma Society during the conduct of the study. All other authors declare no competing interests.

Acknowledgements

This work was supported by grants from Christopher's Smile, Neuroblastoma UK, Cancer Research UK (CRUK) and the National Institute of Health Research (NIHR) Royal Marsden Biomedical Research Centre (BRC).

Supplementary materials

Supplementary material associated with this article can be found, in the online version, at doi:10.1016/j.ebiom.2020.102971.

References

- George SL, Tucker ER, Chesler L. High-Risk Neuroblastoma: current and future therapeutic strategies. *Ann Pediatr Child Health* 2015;3(8):1086.
- Simon T, Hero B, Faldum A, Handgretinger R, Schrappe M, Klingebiel T, et al. Long term outcome of high-risk neuroblastoma patients after immunotherapy with antibody ch14.18 or oral metronomic chemotherapy. *BMC Cancer* 2011;11:21.
- Berthold F, Ernst A, Hero B, Klingebiel T, Kremens B, Schilling FH, et al. Long-term outcomes of the GPOH NB97 trial for children with high-risk neuroblastoma comparing high-dose chemotherapy with autologous stem cell transplantation and oral chemotherapy as consolidation. *Br J Cancer* 2018.
- Garaventa AP, U, Valteau-Couanet D, Castel V, Elliott M, Ash S, Chi-Fung Chan G, Laureys G, Popovik M, Vettenranta K, Balwierz W, Schroeder H, Owens C, Cesen M, Papadakis V, Trahair T, Luksch R, Schleiermacher G, Ambros PF, Ladenstein R. The randomised induction for high-risk neuroblastoma comparing COJEC and N5-MSKCC regimens: early results from the HR-NBL1.5/SIOPEN trial. *J Clin Oncol* 2018;36(suppl); abstr 10507.
- Peifer M, Hertwig F, Roels F, Dreidax D, Gartlgruber M, Menon R, et al. Telomerase activation by genomic rearrangements in high-risk neuroblastoma. *Nature* 2015;526(7575):700–4.
- Valentijn LJ, Koster J, Zwijnenburg DA, Hasselt NE, van Sluis P, Volckmann R, et al. TERT rearrangements are frequent in neuroblastoma and identify aggressive tumors. *Nat Genet* 2015;47(12):1411–4.
- Cheung NK, Zhang J, Lu C, Parker M, Bahrami A, Tickoo SK, et al. Association of age at diagnosis and genetic mutations in patients with neuroblastoma. *JAMA* 2012;307(10):1062–71.
- Grobner SN, Worst BC, Weischenfeldt J, Buchhalter I, Kleinheinz K, Rudneva VA, et al. The landscape of genomic alterations across childhood cancers. *Nature* 2015;526(7575):321–7.
- Cardoso C, Timsit S, Villard L, Khrestchatisky M, Fontes M, Colleaux L. Specific interaction between the XNP/ATR-X gene product and the SET domain of the human *EZH2* protein. *Hum Mol Genet* 1998;7(4):679–84.
- Kovatcheva M, Liao W, Klein ME, Robine N, Geiger H, Crago AM, et al. *ATRX* is a regulator of therapy induced senescence in human cells. *Nat Commun* 2017;8(1):386.
- Law MJ, Lower KM, Voon HP, Hughes JR, Garrick D, Viprakasit V, et al. *ATR-X* syndrome protein targets tandem repeats and influences allele-specific expression in a size-dependent manner. *Cell* 2010;143(3):367–78.
- Goldberg AD, Banaszynski LA, Noh KM, Lewis PW, Elsaesser SJ, Stadler S, et al. Distinct factors control histone variant H3.3 localization at specific genomic regions. *Cell* 2010;140(5):678–91.
- Lewis PW, Elsaesser SJ, Noh KM, Stadler SC, Allis CD. Daxx is an H3.3-specific histone chaperone and cooperates with *ATRX* in replication-independent chromatin assembly at telomeres. *Proc Natl Acad Sci U S A* 2010;107(32):14075–80.

- [14] Clynes D, Jelinska C, Xella B, Ayyub H, Scott C, Mitson M, et al. Suppression of the alternative lengthening of telomere pathway by the chromatin remodelling factor ATRX. *Nat Commun* 2015;6:7538.
- [15] Koschmann C, Calinescu AA, Nunez FJ, Mackay A, Fazal-Salom J, Thomas D, et al. ATRX loss promotes tumor growth and impairs nonhomologous end joining DNA repair in glioma. *Sci Transl Med* 2016;8(328):328ra28.
- [16] Huh MS, Ivanochko D, Hashem LE, Curtin M, Delorme M, Goodall E, et al. Stalled replication forks within heterochromatin require ATRX for protection. *Cell Death Dis* 2016;7:e2220.
- [17] Pugh TJ, Morozova O, Attiyeh EF, Asgharzadeh S, Wei JS, Auclair D, et al. The genetic landscape of high-risk neuroblastoma. *Nat Genet* 2013;45(3):279–84.
- [18] Qadeer ZA, Valle-Garcia D, Hasson D, Sun Z, Cook A, Nguyen C, et al. ATRX In-Frame Fusion Neuroblastoma Is Sensitive to EZH2 Inhibition via Modulation of Neuronal Gene Signatures. *Cancer Cell* 2019;36(5):512–27 e9.
- [19] Bate-Eya LT, Ebus ME, Koster J, den Hartog IJ, Zwijnenburg DA, Schild L, et al. Newly-derived neuroblastoma cell lines propagated in serum-free media recapitulate the genotype and phenotype of primary neuroblastoma tumours. *Eur J Cancer* 2014;50(3):628–37.
- [20] Jabs J, Zickgraf FM, Park J, Wagner S, Jiang X, Jechow K, et al. Screening drug effects in patient-derived cancer cells links organoid responses to genome alterations. *Mol Syst Biol* 2017;13(11):955.
- [21] George SL, Izquierdo E, Campbell J, Koutroumanidou E, Proszek P, Jamal S, et al. A tailored molecular profiling programme for children with cancer to identify clinically actionable genetic alterations. *Eur J Cancer* 2019;121:224–35.
- [22] Zeineldin M, Federico S, Chen X, Fan Y, Xu B, Stewart E, et al. MYCN amplification and ATRX mutations are incompatible in neuroblastoma. *Nat Commun* 2020;11(1):913.
- [23] Haber M, Bordow SB, Gilbert J, Madafoglio J, Kavallaris M, Marshall GM, et al. Altered expression of the MYCN oncogene modulates MRP gene expression and response to cytotoxic drugs in neuroblastoma cells. *Oncogene* 1999;18(17):2777–82.
- [24] Farooqi AS, Dagg RA, Choi LM, Shay JW, Reynolds CP, Lau LM. Alternative lengthening of telomeres in neuroblastoma cell lines is associated with a lack of MYCN genomic amplification and with p53 pathway aberrations. *J Neurooncol* 2014;119(1):17–26.
- [25] Haapaniemi E, Botla S, Persson J, Schmierer B, Taipale J. CRISPR-Cas9 genome editing induces a p53-mediated DNA damage response. *Nat Med* 2018.
- [26] Seah C, Levy MA, Jiang Y, Mokhtarzada S, Higgs DR, Gibbons RJ, et al. Neuronal death resulting from targeted disruption of the Snf2 protein ATRX is mediated by p53. *J Neurosci* 2008;28(47):12570–80.
- [27] Chan DW, Chen BP, Prithivirajasingh S, Kurimasa A, Story MD, Qin J, et al. Auto-phosphorylation of the DNA-dependent protein kinase catalytic subunit is required for rejoining of DNA double-strand breaks. *Genes Dev* 2002;16(18):2333–8.
- [28] Tellli ML, Timms KM, Reid J, Hennessy B, Mills GB, Jensen KC, et al. Homologous recombination deficiency (HRD) score predicts response to platinum-containing neoadjuvant chemotherapy in patients with triple-negative breast cancer. *Clin Cancer Res* 2016;22(15):3764–73.
- [29] Juhasz S, Elbakry A, Mathes A, Loblrich M. ATRX promotes DNA repair synthesis and sister chromatid exchange during homologous recombination. *Mol Cell* 2018;71(1):11–24 e7.
- [30] Birkbak NJ, Wang ZC, Kim JY, Eklund AC, Li Q, Tian R, et al. Telomeric allelic imbalance indicates defective DNA repair and sensitivity to DNA-damaging agents. *Cancer Discov* 2012;2(4):366–75.
- [31] Klusmann I, Rodewald S, Muller L, Friedrich M, Wienken M, Li Y, et al. p53 activity results in DNA replication fork processivity. *Cell Rep* 2016;17(7):1845–57.
- [32] Shen Y, Rehman FL, Feng Y, Boshuizen J, Bajrami I, Elliott R, et al. BMN 673, a novel and highly potent PARP1/2 inhibitor for the treatment of human cancers with DNA repair deficiency. *Clin Cancer Res* 2013;19(18):5003–15.
- [33] Kelland LR, Sharp SY, Rogers PM, Myers TG, Workman P. DT-Diaphorase expression and tumor cell sensitivity to 17-allylamino, 17-demethoxygeldanamycin, an inhibitor of heat shock protein 90. *J Natl Cancer Inst* 1999;91(22):1940–9.
- [34] Reid AH, Protheroe A, Attard G, Hayward N, Vidal L, Spicer J, et al. A first-in-man phase I and pharmacokinetic study on CHR-2797 (Tosedostat), an inhibitor of M1 aminopeptidases, in patients with advanced solid tumors. *Clin Cancer Res* 2009;15(15):4978–85.
- [35] Liu X, Jiang Y, Nowak B, Qiang B, Cheng N, Chen Y, et al. Targeting BRCA1/2 deficient ovarian cancer with CNDAC-based drug combinations. *Cancer Chemother Pharmacol* 2018;81(2):255–67.
- [36] Sun L, Liang C, Shirazian S, Zhou Y, Miller T, Cui J, et al. Discovery of 5-[5-fluoro-2-oxo-1,2-dihydroindol-(3Z)-ylidenemethyl]-2,4-dimethyl-1H-pyrrole-3-carboxylic acid (2-diethylaminoethyl)amide, a novel tyrosine kinase inhibitor targeting vascular endothelial and platelet-derived growth factor receptor tyrosine kinase. *J Med Chem* 2003;46(7):1116–9.
- [37] Xu Y, Villalona-Calero MA, Irinotecan. mechanisms of tumor resistance and novel strategies for modulating its activity. *Ann Oncol* 2002;13(12):1841–51.
- [38] Bryant HE, Petermann E, Schultz N, Jemth AS, Loseva O, Issaeva N, et al. PARP is activated at stalled forks to mediate Mre11-dependent replication restart and recombination. *EMBO J* 2009;28(17):2601–15.
- [39] Stewart E, Goshorn R, Bradley C, Griffiths LM, Benavente C, Twarog NR, et al. Targeting the DNA repair pathway in Ewing sarcoma. *Cell Rep* 2014;9(3):829–41.
- [40] Pujade-Lauraine E, Ledermann JA, Selle F, Gebski V, Penson RT, Oza AM, et al. Olaparib tablets as maintenance therapy in patients with platinum-sensitive, relapsed ovarian cancer and a BRCA1/2 mutation (SOLO2/ENGOT-Ov21): a double-blind, randomised, placebo-controlled, phase 3 trial. *Lancet Oncol* 2017;18(9):1274–84.
- [41] Robson M, Im SA, Senkus E, Xu B, Domchek SM, Masuda N, et al. Olaparib for metastatic breast cancer in patients with a germline BRCA mutation. *N Engl J Med* 2017;377(6):523–33.
- [42] Liu XJ, Nowak B, Wang YQ, Plunkett W. Sapacitabine, the prodrug of CNDAC, is a nucleoside analog with a unique action mechanism of inducing DNA strand breaks. *Chin J Cancer* 2012;31(8):373–80.
- [43] Watson LA, Solomon LA, Li JR, Jiang Y, Edwards M, Shin-ya K, et al. Atrx deficiency induces telomere dysfunction, endocrine defects, and reduced life span. *J Clin Invest* 2013;123(5):2049–63.
- [44] Hong DS, Banerji U, Tavana B, George GC, Aaron J, Kurzrock R. Targeting the molecular chaperone heat shock protein 90 (HSP90): lessons learned and future directions. *Cancer Treat Rev* 2013;39(4):375–87.
- [45] Choi YE, Battelli C, Watson J, Liu J, Curtis J, Morse AN, et al. Sublethal concentrations of 17-AAG suppress homologous recombination DNA repair and enhance sensitivity to carboplatin and olaparib in HR proficient ovarian cancer cells. *Oncotarget* 2014;5(9):2678–87.
- [46] Pennisi R, Antocchia A, Leone S, Ascenzi P, di Masi A. Hsp90alpha regulates ATM and NBN functions in sensing and repair of DNA double-strand breaks. *FEBS J* 2017;284(15):2378–95.
- [47] Stecklein SR, Kumaraswamy E, Behbod F, Wang W, Chaguturu V, Harlan-Williams LM, et al. BRCA1 and HSP90 cooperate in homologous and non-homologous DNA double-strand-break repair and G2/M checkpoint activation. *Proc Natl Acad Sci U S A* 2012;109(34):13650–5.
- [48] Li Y, Seto E. HDACs and HDAC inhibitors in cancer development and therapy. *Cold Spring Harb Perspect Med* 2016;6(10).
- [49] Loponte S, Segre CV, Senese S, Miccolo C, Santaguida S, Deflorian G, et al. Dynamic phosphorylation of Histone Deacetylase 1 by Aurora kinases during mitosis regulates zebrafish embryos development. *Sci Rep* 2016;6:30213.
- [50] Brockmann M, Poon E, Berry T, Carstensen A, Deubzer HE, Rycak L, et al. Small molecule inhibitors of aurora-a induce proteasomal degradation of N-myc in childhood neuroblastoma. *Cancer Cell* 2013;24(1):75–89.
- [51] Norris RE, Adamson PC, Nguyen VT, Fox E. Preclinical evaluation of the PARP inhibitor, olaparib, in combination with cytotoxic chemotherapy in pediatric solid tumors. *Pediatr Blood Cancer* 2014;61(1):145–50.